

Identifying Sky Conditions in Iran from MODIS Terra and Aqua Cloud Products

Khodakaram HATAMI BAHMANBEIGLOU, Saeed MOVAHEDI

(*Faculty of Geographical Sciences and Planning, University of Isfahan, Isfahan 81746-73441, Iran*)

Abstract: Clouds can influence climate through many complex interactions within the hydrological cycle. Due to the important effects of cloud cover on climate, it is essential to study its variability over certain geographical areas. This study provides a spatial and temporal distribution of sky conditions, cloudy, partly cloudy, and clear days, in Iran. Cloud fraction parameters were calculated based on the cloud product (collection 6_L2) obtained from the Moderate Resolution Imaging Spectroradiometer (MODIS) sensors on board the Terra (MOD06) and Aqua (MYD06) satellites. The cloud products were collected daily from January 1, 2003 to December 31, 2014 (12 years) with a spatial resolution of 5 km × 5 km. First, the cloud fraction data were converted into a regular geographic coordinate network over Iran. Then, the estimations from both sensors were analyzed. Results revealed that the maximum annual frequency of cloudy days occurs along the southern shores of the Caspian Sea, while the minimum annual frequency occurs in southeast Iran. On average, the annual number of cloudy and clear-sky days was 88 and 256 d from MODIS Terra, as compared to 96 and 244 d from MODIS Aqua. Generally, cloudy and partly cloudy days decrease from north to south, and MODIS Aqua overestimates the cloudy and partly cloudy days compared to MODIS Terra.

Keywords: cloud fraction; sky conditions; Moderate Resolution Imaging Spectroradiometer (MODIS); Terra satellite; Aqua satellite; Iran

Citation: Bahmanbeiglou Khodakaram Hatami, Movahedi Saeed, 2017. Identifying sky conditions in Iran from MODIS Terra and Aqua cloud products. *Chinese Geographical Science*, 27(5): 800–809. doi: 10.1007/s11769-017-0908-4

1 Introduction

Among other meteorological parameters, cloudiness is often considered one of the most useful phenomena for monitoring climate system changes (Filipiak and Miettus, 2009). Clouds, which display a great variability in space, time, and type, can influence climate through many complex interactions within the hydrological cycle. Clouds play a dominant role in controlling radiative fluxes in the atmosphere (Schiffer and Rossow, 1983) and have an important controlling influence on the radiation balance (Griggs and Bamber, 2008). They are also the strongest modulator of the solar radiant energy

absorbed by the earth atmosphere system due to their large spatial and temporal variability (Chen *et al.*, 2012; 2016). Previous studies have shown that clouds and precipitation have feedbacks related to aerosol pollution in developing countries, such as China (Guo *et al.*, 2011; 2016a; Li *et al.*, 2016) and India (Ramanathan *et al.*, 2001). The distribution of clouds remains elusive due to complicated aerosol-cloud interactions (Koren *et al.*, 2014; Wang *et al.*, 2014; 2015). Clouds in turn affect the development of planetary boundary layer (Guo *et al.*, 2016b), which further exerts an non-negligible effect on the geographic discrepancy of global warming (Davy and Esau, 2016).

Received date: 2017-01-13; accepted date: 2017-05-04

Foundation item: Under the auspices of Faculty of Geographical Science and Planning, University of Isfahan, Doctoral Climatology Project (No. 168607/94)

Corresponding author: Saeed MOVAHEDI. E-mail: S.movahedi@geo.ui.ac.ir

© Science Press, Northeast Institute of Geography and Agroecology, CAS and Springer-Verlag Berlin Heidelberg 2017

When quantified globally at high spatial resolution, cloud cover dynamics can provide key information for delineating a variety of habitat types and predicting species distributions (Wilson and Jetz, 2016). Many cross-disciplinary studies have been conducted to research cloud cover impacts on the natural world. For instance, some researchers have described the importance of cloud cover in conjunction with radiant fluxes (e.g., Spena *et al.*, 2010; Chen *et al.*, 2012). Others have examined the spatial distribution of cloud cover on a global scale; Clouds are most frequently found in the intertropical convergence zone (ITCZ) and the mid-latitude storm belts of the North Atlantic, North Pacific, and Antarctic. In between are the subtropical high pressure zones over the oceans and the subtropical deserts over land where clouds are less frequent (Wylie *et al.*, 2005; Pincus *et al.*, 2012; King *et al.*, 2013). The trend in cloud cover has been widely investigated on both global and regional scales. In recent years, cloud cover has decreased over East Asia (Wu and Liu, 2013) and China (Xia, 2012). Similarly, a pronounced decreasing trend has been observed over the western regions of the United States, while there is increasing cloud cover over western Canada, the eastern regions of the United States, and Baffin Island (Tang and Leng, 2013). A large decrease in cloud cover over South America, small decrease in cloud cover over Eurasia and Africa, and no trend over North America have also been reported (Warren *et al.*, 2007). Additionally, although the annual average cloud cover appears to be increasing in Amazonia, there is a distinct seasonality, with a significant decrease in the dry season and increase in the wet season (Butt *et al.*, 2009). Arctic clouds change differently from land to ocean, but the overall trend from 1971 to 2007 showed a slight increase in total cloud cover during all seasons (Eastman and Warren, 2010). In Iran, the maximum spatial changes in cloud cover appear in the southern shores of the Caspian Sea and minimum spatial changes in southern Iran; overall cloud coverage has exhibited a decreasing trend (Rasooli *et al.*, 2013). Furthermore, overcast days have been decreasing and clear days have been increasing in northeast Iran; these data are based on weather station data from Sabzevar, Torbate Heydarie, and Birjand, and there is a reversed trend at Mashhad station (Bannayan *et al.*, 2011).

On a regional scale, investigating cloud cover using synoptic meteorological data is routine in climatology; it

has been used in Japan (Nakamura *et al.*, 1985), Spain (Garcia *et al.*, 2008), Poland (Filipiak and Mietus, 2009), Sweden (Congren, 2013), and eastern Romania (Bostan *et al.*, 2015) to identify spatial and temporal distributions of cloud cover. In addition, the ISCCP D2 global data archive, which includes monthly mean properties of cloud with $2.5^\circ \times 2.5^\circ$ spatial resolution, and surface observations were used to investigate cloud cover over China (Li *et al.*, 2004). However, remote sensing data for long period and high resolution studies have been seldom used.

The objective of this paper is to present a procedure for applying MODIS cloud product data at high-resolution to a regional scale study. MODIS cloud product data are not provided in a standard geographical coordinate system, e.g., Mosaic packing, at 5-km and 1-km spatial resolutions. Therefore, converting the data to a standard coordinate system at a regional scale is an additional feature of this research. Global scale data with the spatial resolution of $1^\circ \times 1^\circ$ (MOD08_D3; MYD08_D3) have been provided from MODIS cloud products (MOD06_L2; MYD06-L2) (Platnick *et al.*, 2014), however, these data are at a low spatial resolution.

This paper is organized as follows. In the subsequent, second section, approaches for converting data to a standard coordinate system and classifying sky conditions to quantify cloud information are proposed. These sky condition classifications are important for designing energy-efficient and sustainable buildings, and predicting their energy consumption and daylight performance. Sky conditions are commonly classified into overcast, partly cloudy, and clear sky (Kong and Kim, 2013). In the third section, we evaluate the spatial distribution of sky conditions and their annual mean. Then, we compare two datasets (Aqua and Terra) and sky conditions trends across Iran. Finally, the main conclusions and implemented procedures are summarized in the final section.

2 Materials and Methods

2.1 Study area

The study area is the country of Iran (25°N – 40°N , 44°E – 63°E), a mountainous country bordering the Oman Sea, Persian Gulf, and Caspian Sea (Javanmard *et al.*, 2010) (Fig. 1). Iran hosts a variety of climates,

which are divided as follows: 35.5% hyper-arid, 29.2% arid, 20.1% semi-arid, 5% Mediterranean, and 10% wet, i.e., cold mountainous type. Therefore, > 82% of Iran's territory is located in the arid and semi-arid climate zone. The mean annual precipitation in Iran is about 250 mm, which is less than one third of the mean annual global precipitation, 860 mm. In addition, this sparse precipitation is also unfavorable temporally and spatially, and severe drought is recognized as a feature of Iran's climate (Amiri and Eslamian, 2010). Another important climatic element is extreme temperature changes, which can range from -20°C to 50°C .

2.2 MODIS data

MODIS is a 36-band whisk-broom-scanning radiometer currently flying on the National Aeronautics and Space Administration (NASA) Terra and Aqua platforms (Menzel *et al.*, 2008). Aqua and Terra provide global coverage every 1–2 d; therefore, they provide an important global dataset of cloud properties for climate and cloud process studies (King *et al.*, 2013). In this study, we use cloud fraction parameters from the MODIS cloud product (L2), which are archived in a self-described hierarchical data format (HDF). A 5-min file or granule contains earth-located data ranging from approximately 2330 km cross-track (1354 1-km pixels) to 2000 km along-track. The Terra overpass time at the Equator is around 10:30 and 22:30 local solar time in its descending (daytime) and ascending (nighttime) modes, respectively. The Aqua overpass time is around 13:30 and 1:30 local solar time in its ascending (daytime) and

descending (nighttime) modes, respectively (Platnick *et al.*, 2014). In Collection 6, cloud products are provided at both 1-km and 5-km resolutions (Menzel *et al.*, 2013). The cloud fraction parameter is computed from a cloud mask product. The cloud mask cloudiness flag has the following settings: 0 = confidently cloudy, 1 = probably cloudy, 2 = probably clear, and 3 = confidently clear. In the computation of cloud fraction, the first two flags are assigned 100% cloudy, and the last two flags are assigned 100% clear. Therefore, cloud fractions have values of 0, 4%, 8%, 12%, and 16% to 100% in cloud product L2 at 5 km \times 5 km resolution. Terra (Aqua) uses a MOD (MYD) prefix (Hubanks *et al.*, 2015). We downloaded both sets of daily satellite cloud product data over Iran from the website: <ftp://ladsftp.nascom.nasa.gov/> for the period from January 1, 2003 to December 31, 2014. Then, we selected the cloud fraction parameters from both satellites to analyze sky conditions over Iran.

2.3 Methods

2.3.1 Converting cloud fraction data to a standard coordinate system

A regular network on a global scale with the spatial resolution of $1^{\circ} \times 1^{\circ}$ (MOD08-D3; MYD08-D3) has been provided for MODIS cloud products (Platnick *et al.*, 2014), but it is inappropriate for regional studies. MODIS cloud products from the Terra and Aqua satellites (MOD06 and MYD06, respectively) are not provided in a regular geographical coordinate system (Mosaic packing) at 5-km and 1-km spatial resolutions. Therefore, it is essential that the desired parameter data be transferred to a regular coordinate system by applying appropriate methods. We applied a new method to transfer cloud fraction data to a standard coordinate system based on the geographical coordinate system for Iran. First, a network of geographical coordinates with spatial resolution arrays of 5 km \times 5 km, based on the framework for Iran was prepared as a standard grid with dimensions of 353 \times 618 pixels (353 rows and 618 columns). Subsequently, the data in the granule were transferred to the standard grid over Iran for each day. A radius of approximately 7.5 km was applied as a fixed coordinate around each pixel in the standard grid. Then, the coordinates of MODIS granules, which lay within this radius, were selected, and according to the nearest distance method, one cloud fraction value was transmit-

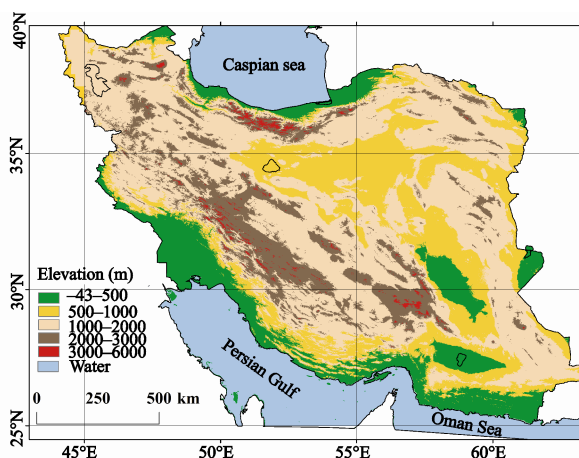


Fig. 1 Map of the Iran study area indicating the location between the Caspian Sea, Persian Gulf, and Oman Sea, and showing a Digital Elevation Model (DEM) of terrain

ted to the pixel in the standard grid. Therefore, for each day during the study period, cloud fraction data projected on a standard grid were obtained.

2.3.2 Sky conditions classification

Sky conditions are defined as the descriptions of the appearance of sky and can be evaluated either automatically with instruments or manually with or without instruments (U.S. Department of Commerce/National Oceanic and Atmospheric Administration, 1995). In this study, to identify sky conditions over Iran, cloud fraction data (Terra and Aqua) were classified as follows: cloud fractions 0% to 25.0% (0–2 oktas) were defined for clear days, 25.0% to 62.5% for partly cloudy days (2–5 oktas), and 62.5% to 100.0% (5–8 oktas) for cloudy days. One okta is equal to 12.5% cloud fraction (Kotarba, 2009). Data obtained from the Terra satellite (morning and evening time) and Aqua satellite (night and forenoon) were separately combined daily. Subsequent to combining the data, the frequency of sky conditions was estimated at monthly and annual time scales over Iran. Many researchers have used different approaches to classify sky conditions, but no consensus has been reached on classification in this discipline. Therefore, the classifications provided here manifest the spatial and temporal distributions of sky conditions and are in general agreement with the classifications defined by Dai *et al.* (1999), Xia (2012), Bannayan *et al.* (2011), and Calbo and Sabburg (2008).

2.3.3 Analysis of sky condition trends

According to data availability, we calculated the spatial distribution of sky conditions trends for the period 2003–2014. To identify spatial trends, we applied a confidence interval (CI) for the slope of a simple linear regression model with 95% confidence levels.

3 Results and Discussion

3.1 Long-term climatological features

The long-term means of sky condition classifications for Iran were calculated. The frequencies of cloudy and partly cloudy days were respectively calculated as 88 and 21 d based on the Terra satellite data and 96 and 25 d based on the Aqua satellite data. The frequency of clear days was 256 d and 244 d based on Terra and Aqua satellite data, respectively. Overall, the Aqua satellite provided larger numbers of calculated cloudy and partly cloudy days compared to the Terra satellite (Table 1).

Table 1 Long-term average of sky condition classification (d)

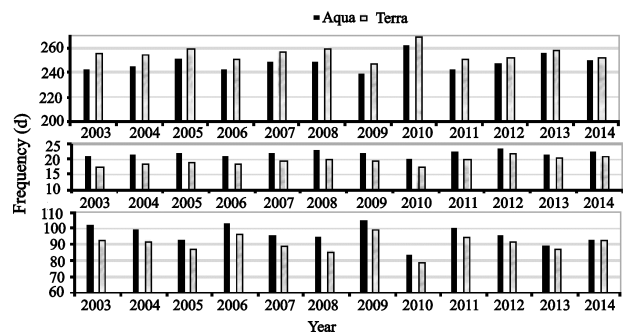
Satellite	Number of cloudy days	Number of partly cloudy days	Number of clear days
Terra	88	21	256
Aqua	96	25	244

Data from both satellites indicated that the maximum monthly frequency of cloudy days was 14 d, which occurred in January. In contrast, the minimum monthly frequency of cloudy days was different between satellite data sets, occurring in September based on Aqua satellite data, and in August and September based on Terra satellite data. The maximum monthly frequency of clear days in the Aqua satellite data was approximately 27 d, which largely occurred in August, September, and July. The frequency was 28 d in August based on Terra satellite data. The minimum monthly frequency of clear days was 13 d, in January and February, based on Aqua satellite data. In contrast, the frequency of clear days increased in these months and reached 14 d per month based on Terra satellite data. The maximum monthly frequency of partly cloudy days occurred in January, 4 d, based on Aqua satellite data, but it was 3 d in January and September based on Terra satellite data. The minimum monthly partly cloudy days from both satellites occurred in July and continued to October. The review of standard deviation data per monthly period indicated that the standard deviation from both satellites was 3.2–4.9 d on clear days, 2.6–4.9 d on cloudy days, and 0.9–1.6 d on partly cloudy days. Accordingly, partly cloudy days had the minimum data dispersion compared to clear and cloudy days, and data dispersion was not significantly different between cloudy days and partly cloudy days from the individual satellite data (Table 2).

Annual frequencies of sky conditions calculated using data from both satellites from 2003 to 2014 over Iran are shown in Figs. 2a, 2b, and 2c. As shown, the maximum frequency of clear and cloudy days occurred in 2010 and 2009 based on Aqua satellite data; additionally, the maximum occurrence of clear days based on Terra and Aqua satellite data was similar in 2000. The annual frequency of partly cloudy days from data from both satellites showed that the minimum and maximum number of partly cloudy days occurred in 2010 and 2012, respectively. In total, the annual frequency of cloudy days, clear days and partly cloudy days was 79(83)–99(104) d, 247(239)–269(262) d and 18–24 d

Table 2 Monthly frequency (Freq) and standard deviation (STD) of cloudy, partly cloudy, and clear days

Month	Aqua satellite						Terra satellite					
	Clear days		Partly cloudy days		Cloudy days		Clear days		Partly cloudy days		Cloudy days	
	Freq	STD	Freq	STD	Freq	STD	Freq	STD	Freq	STD	Freq	STD
January	13	4.4	4	1.5	14	4.9	14	4.2	3	1.6	14	4.7
February	13	4.3	2	1.5	13	4.8	14	4.0	2	1.5	12	4.4
March	17	4.7	2	1.4	12	4.1	18	4.5	2	1.4	11	4.9
April	17	4.8	2	1.2	11	4.4	17	3.7	2	1.1	11	4.3
May	21	4.2	2	1.3	8	4.6	22	4.1	2	1.2	7	4.5
June	25	3.9	2	1.1	3	3.2	26	3.6	1	0.9	3	3.0
July	27	4.0	1	1.1	3	3.4	27	3.7	1	1.0	3	3.1
August	27	3.6	1	1.1	3	3.0	28	3.2	1	0.9	2	2.6
September	27	3.8	1	1.0	2	3.2	27	3.4	1	0.9	2	2.9
October	25	4.8	1	1.2	5	4.1	25	3.5	1	1.1	5	3.9
November	18	4.4	2	1.3	10	4.8	19	4.2	2	1.3	9	4.6
December	16	4.8	3	1.6	12	4.4	16	4.5	3	1.6	12	4.9

**Fig. 2** Annual frequency of clear days (a), partly cloudy days (b), and cloudy days (c) based on data from the Terra and Aqua satellites

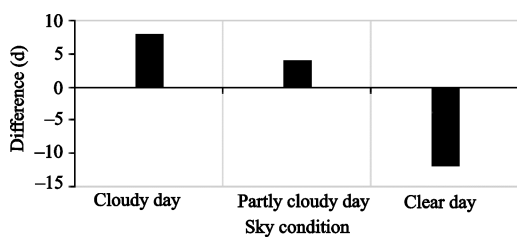
for Terra (Aqua) satellite data. Generally, MODIS Aqua data overestimated the cloudy and partly cloudy days compared to MODIS Terra data.

MODIS Aqua data overestimated the long-term mean of cloudy and partly cloudy days compared to MODIS Terra (Fig. 3) data. This difference between the data from the two sensors is possibly due to the differences in the sensor design and time differences between the satellite over passes (Kumar *et al.*, 2015).

3.2 Spatial distribution of sky conditions

The spatial distribution of sky conditions, cloudy, partly cloudy, and clear days, in Iran was evaluated separately for the Terra and Aqua satellite data. The annual frequency of cloudy day spatial distributions from Terra and Aqua satellite data (Figs. 4a and 4b) demonstrates that the maximum occurrence of cloudy days occurred

along the southern shores of the Caspian Sea, which is consistent with the findings of Rasooli *et al.* (2013) and Alijani (1995); in this region, Terra satellite data estimated cloudy days for up to 239 d and Aqua satellite data estimated cloudy days up to 255 d. Data from both satellites indicated that the minimum number of cloudy days were observed in southeast Iran, Terra and Aqua satellite data estimates were as low as 35 and 37 d, respectively. The maximum occurrence of partly cloudy days (40–58 d) were in the high elevation Alborz Mountain based on Terra satellite data and in the high elevation Zagros Mountain based on Aqua satellite data. The minimum annual frequency of partly cloudy days based on data from both satellites was < 10 d, and observed in southeast Iran (Figs. 4c and 4d). The annual frequency of spatial distribution of clear days, according to Terra and Aqua satellite data (Figs. 4e and 4f) indicated that the regions with maximum clear days generally occurred in south and southeast Iran. Furthermore,

**Fig. 3** Differences in the mean annual frequency of calculated sky conditions between the Terra and Aqua satellite data. Positive values indicate that Aqua data estimated more clouds than Terra data

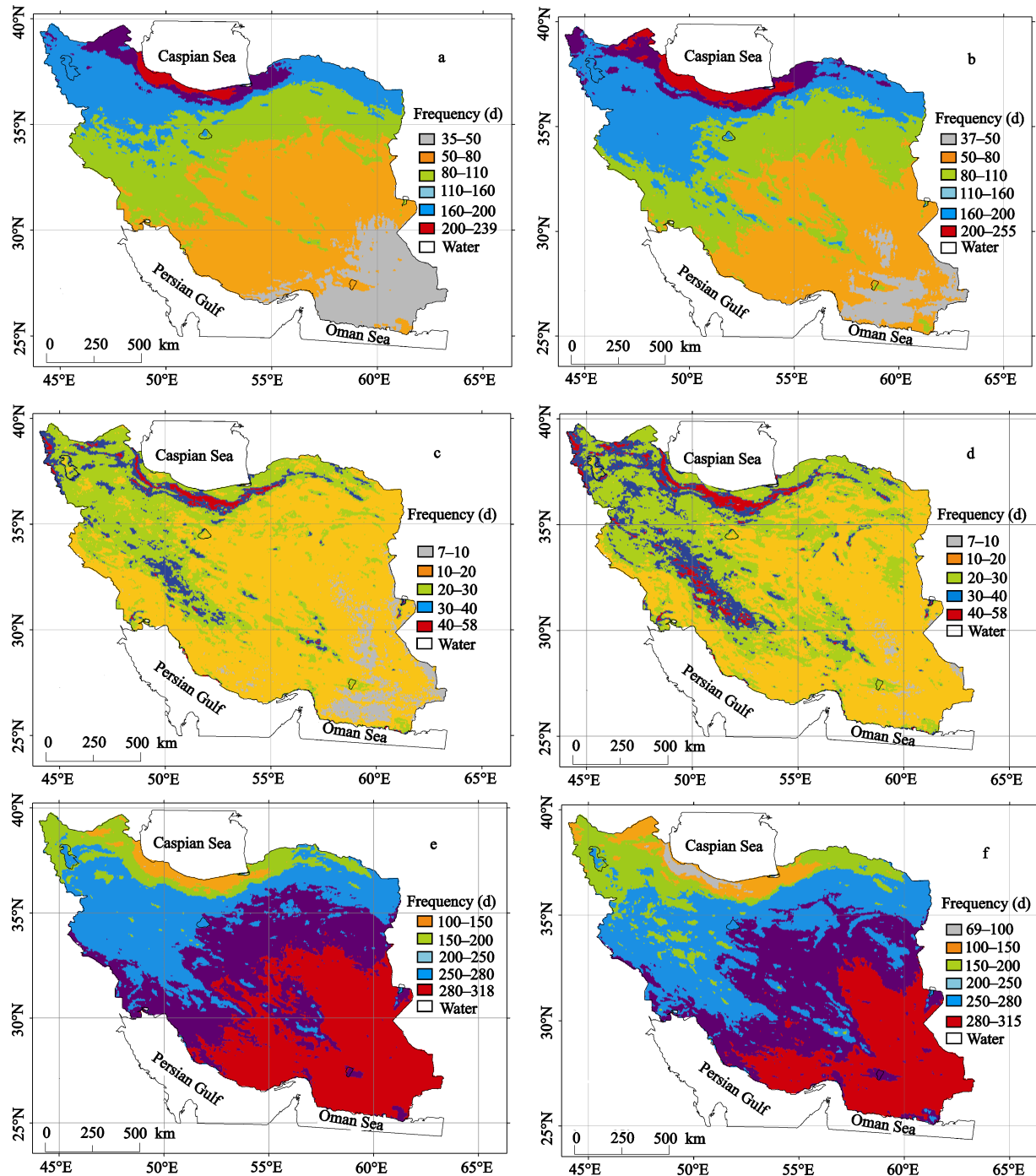


Fig. 4 Spatial distribution of annual cloudy day frequency based on data from Terra (a) and Aqua (b), partly cloudy day frequency from Terra (c) and Aqua (d), and clear day frequency from Terra (e) and Aqua (f)

the minimum clear days based on both sets of satellite data were observed along the southern shores of the Caspian Sea, where the Terra satellite recorded more clear days (100–150 d) than the Aqua satellite (69–100 d).

The sky conditions were calculated based on the total land areas of the country according to the Terra and Aqua satellite data (Table 3). The estimates indicated

that cloudy days for more than 200 d covered more than 1.1% (2.5%) of the country according to Terra (Aqua) satellite data. Cloudy days for 50–80 d covered 39.1% (36.0%) of the country based on Terra (Aqua) satellite data. Partly cloudy days for 7–10 d covered 5.1% (0.9%) based on Terra (Aqua) satellite data. In comparison, partly cloudy days for 10–20 d covered 59.3%

(48.4%) of total land area according to Terra (Aqua) satellite data. Clear days for > 280 d covered 32.9% (22.9%) of total area based on Terra (Aqua) satellite data. However, both satellites indicated that > 200 clear days covered approximately 85% of the land area of Iran; generally, cloud coverage was very weak in most regions of Iran.

3.3 Analysis of sky condition trends

We employed a simple linear regression to compute pixel-based trends in Iran. Slope values less than -0.1 d were defined as decreasing trends, between -0.1 and 0.1 d were defined as no trend, and more than 0.1 d were defined as increasing trends. The annual spatial trend on clear days for both sets of satellite data (Terra and Aqua) indicated that the number of clear days had an increasing trend along the eastern shores of the Caspian Sea and parts of south and northeast Iran; however, there were no other trends in other parts of the country (Figs. 5a and 5b). The cloudy day trends from both satellite data sets indicated a decreasing trend along the eastern shores of the Caspian Sea and parts of south and northeast Iran, while there were no trends in other parts of the country (Figs. 5c and 5d). The annual trends for partly cloudy days from both sets of satellite data showed increasing trends for mountain tops, while other parts of the country had no trends (Figs. 5e and 5f).

4 Conclusions

In this study, we analyzed the spatial and temporal characteristics of cloud coverage over Iran, based on classification methods for sky conditions (partly cloudy, cloudy, and clear days) developed here. In particular, we selected cloud fraction parameters from MODIS sensors

on the board Terra (MOD06) and Aqua (MYD06) satellites. Because level 2 Collection 6 cloud products from MODIS were not transformed to a standard coordinate grid at high spatial resolution, 1-km or 5-km, we first transformed the cloud fraction parameter data at 5 km \times 5 km resolution to the standard grid for Iran, daily and at 5 km \times 5 km resolution. Using this gridded data, trends in cloud fraction were evaluated for a 12-year time period. We first classified sky conditions using the following criteria: 0–26.0% for clear, 26.0%–62.5% for partly cloudy, and 62.5%–100.0% for cloudy days. Subsequently, we analyzed the spatial and temporal distributions of different sky conditions over Iran. Results revealed that the average frequency of cloudy days was approximately 88(96) d for Terra (Aqua) satellite data compared to 244(256) d for clear day frequency. Maximum cloudy days tended to occur along the southern parts of the Caspian Sea, up to 240(255) d based on Terra (Aqua) satellite data. Both satellites recorded maximum clear day frequencies in south and southeast Iran, at more than 280 d. Generally, Aqua data provided higher estimates of cloudy and partly cloudy days than Terra data; this is due to differences in pass over times and sensor designs. However, the spatial pattern of cloudy, partly cloudy, and clear days recorded by both satellites were structurally almost identical, which suggests that they have similar capabilities for revealing cloud cover over Iran. More generally, the frequency of cloudy days decreased from north to south, indicating that the spatial distribution of sky condition trends were not the same regionally. This diversity of cloud cover spatial patterns and trends can be attributed to different climatic systems entering the country, global climate change, and the considerable latitude extension from northern to southern Iran.

Table 3 Percentages of land areas with different sky conditions and their frequency

Land area with cloudy days			Land area with partly cloudy days			Land area with clear days		
Frequency range (d)	Terra (%)	Aqua (%)	Frequency range (d)	Terra (%)	Aqua (%)	Frequency range (d)	Terra (%)	Aqua (%)
<50	13.1	6.2	7–10	5.1	0.9	<100	0.0	0.9
50–80	39.1	36.0	10–20	59.3	48.4	100–150	2.5	4.2
80–110	26.3	28.0	20–30	27.2	35.9	150–200	7.8	11.9
110–160	16.8	22.5	30–40	6.6	11.9	200–250	27.2	30.7
160–200	3.6	4.8	>40	1.8	2.8	250–280	29.6	29.5
>200	1.1	2.5				>280	32.9	22.9

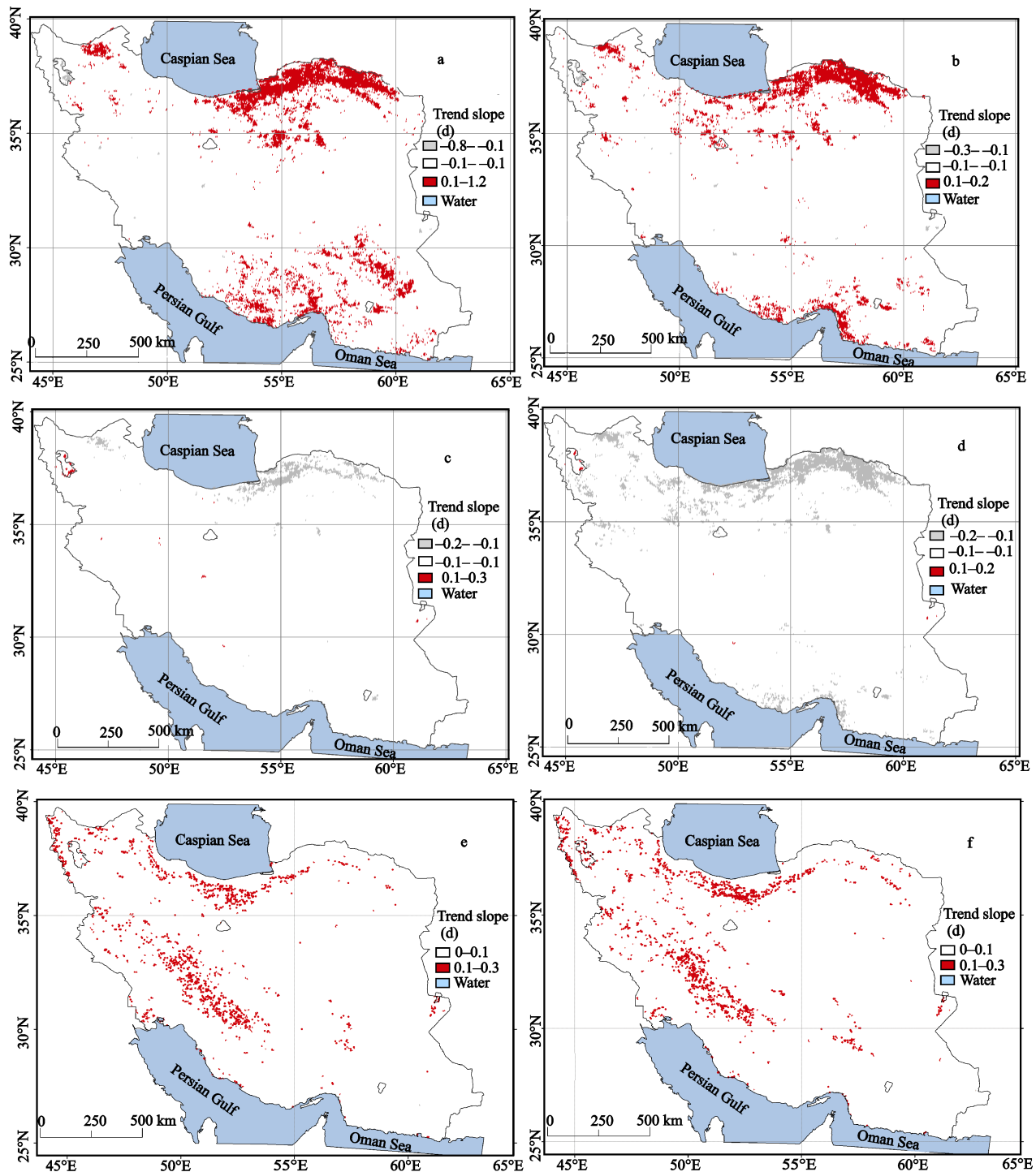


Fig. 5 Spatio-temporal trends in annual number of clear days with Terra (a) and Aqua (b), cloudy days with Terra (c) and Aqua (d), and partly cloudy days with Terra (e) and Aqua (f) satellite data

References

- Alijani B, 1995. *Climate of Iran*. Tehran: Payame Noor Publications, 236.
- Amiri M J, Eslamian S S, 2010. Investigation of climate change in Iran. *Journal of Environmental Science and Technology*, 3(4): 208–216. doi: 10.3923/jest.2010.208.216
- Bannayan A M, Mohamadian A, Alizadeh A, 2011. On climate variability in north east of Iran. *Journal of Water and Soil*, 24(1): 118–131.
- Bostan D C, Manea E F, Stefan S, 2015. Total and partial cloudiness distribution in eastern Romania. *Romanian Reports in*

- Physics*, 67(3): 1117–1127.
- Butt N, New M, Lizcano G *et al.*, 2009. Spatial patterns and recent trends in cloud fraction and cloud-related diffuse radiation in Amazonia. *Journal of Geophysical Research: Atmospheres*, 114(D21): D21104. doi: 10.1029/2009JD012217
- Calbo J, Sabburg J, 2008. Feature extraction from whole-sky ground-based images for cloud-type recognition. *Journal of Atmospheric and Oceanic Technology*, 25(1): 3–14. doi: 10.1175/2007JTECHA959.1
- Chen L, Yan G J, Wang T X *et al.*, 2012. Estimation of surface shortwave radiation components under all sky conditions: modeling and sensitivity analysis. *Remote Sensing of Environment*, 123: 457–469. doi: 10.1016/j.rse.2012.04.006
- Chen T M, Guo J P, Li Z Q *et al.*, 2016. A CloudSat perspective on the cloud climatology and its association with aerosol perturbations in the vertical over Eastern China. *Journal of the Atmospheric Sciences*, 73(9): 3599–3616. doi: 10.1175/JAS-D-15-0309.1
- Congren C, 2013. *Spatial and Temporal Variation of Cloud Free Days in Sweden*. Gothenburg: University of Gothenburg, 1–26.
- Dai A G, Trenberth K E, Karl T R, 1999. Effects of clouds, soil moisture, precipitation, and water vapor on diurnal temperature range. *Journal of Climate*, 12(8): 2451–2473. doi: 10.1175/1520-0442(1999)012<2451:EOCSMP>2.0.CO;2
- Davy R, Esau I, 2016. Differences in the efficacy of climate forcings explained by variations in atmospheric boundary layer depth. *Nature Communications*, 7: 11690. doi: 10.1038/ncomms11690
- Eastman R, Warren G S, 2010. Interannual variations of arctic cloud types in relation to sea ice. *Journal of Climate*, 23(15): 4216–4223. doi: 10.1175/2010JCLI3492.1
- Filipiak J, Miętus M, 2009. Spatial and temporal variability of cloudiness in Poland, 1971–2000. *International Journal of Climatology*, 29(9): 1294–1311. doi: 10.1002/joc.1777
- Garcia P, Benarroch A, Riera J M, 2008. Spatial distribution of cloud cover. *International Journal of Satellite Communications and Networking*, 26(2): 141–155. doi: 10.1002/sat.899
- Griggs J, Bamber J, 2008. Assessment of cloud cover characteristics in satellite datasets and reanalysis products for Greenland. *Journal of Climate*, 21(9): 1837–1849. doi: 10.1175/2007JCLI1570.1
- Guo J P, Zhang X Y, Wu Y R *et al.*, 2011. Spatio-temporal variation trends of satellite-based aerosol optical depth in China during 1980–2008. *Atmospheric Environment*, 45(37): 6802–6811. doi: 10.1016/j.atmosenv.2011.03.068
- Guo J P, Deng M J, Lee S S *et al.*, 2016a. Delaying precipitation and lightning by air pollution over the Pearl River Delta. Part I: Observational analyses. *Journal of Geophysical Research: Atmospheres*, 121(11): 6472–6488. doi: 10.1002/2015JD023257
- Guo J P, Miao Y C, Zhang Y *et al.*, 2016b. The climatology of planetary boundary layer height in China derived from radiosonde and reanalysis data. *Atmospheric Chemistry and Physics*, 16(20): 13309–13319. doi: 10.5194/acp-16-13309-2016
- Hubanks P, Platnick S, King M *et al.*, 2015. MODIS atmosphere L3 gridded product algorithm theoretical basis document (ATBD) & users guide. ATBD reference number ATBDMOD-30, NASA. Available at: https://modis-atmos.gsfc.nasa.gov/_docs/L3_ATBD_C6_2015_05_06.pdf. Cited 6 May 2015
- Javanmard S, Yatagai A, Nodzu M I *et al.*, 2010. Comparing high-resolution gridded precipitation data with satellite rainfall estimates of TRMM_3B42 over Iran. *Advances in Geosciences*, 25: 119–125. doi: 10.5194/adgeo-25-119-2010
- King N J, Bower K N, Crosier J *et al.*, 2013. Evaluating MODIS cloud retrievals with in situ observations from VOCALS-Rex. *Atmospheric Chemistry and Physics*, 13(1): 191–209. doi: 10.5194/acp-13-191-2013
- Kong H J, Kim J T, 2013. A Classification of real sky conditions for Yongin, Korea. In: Hakansson A *et al.* (eds). *Sustainability in Energy and Buildings*. Smart Innovation, Systems and Technologies, vol 22. Berlin, Heidelberg: Springer.
- Koren I, Dagan G, Altaratz O, 2014. From aerosol-limited to invigoration of warm convective clouds. *Science*, 344(6188): 1143–1146. doi: 10.1126/science.1252595
- Kotarba A Z, 2009. A comparison of MODIS-derived cloud amount with visual surface observations. *Atmospheric Research*, 92(4): 522–530. doi: 10.1016/j.atmosres.2009.02.001
- Kumar S V V A, Babu K N, Shukla A K, 2015. Comparative analysis of chlorophyll-a distribution from SEAWIFS, MODIS-AQUA, MODIS-TERRA and MERIS in the Arabian Sea. *Marine Geodesy*, 38(1): 40–57. doi: 10.1080/01490419.2014.914990.
- Li Z, Cribb M C, Chang F L *et al.*, 2004. Validation of MODIS-retrieved cloud fractions using whole sky imager measurements at the three ARM sites. *Proceedings of the 14th ARM Science Team Meeting*. Albuquerque, New Mexico: ARM.
- Li Z Q, Lau W K M, Ramanathan V *et al.*, 2016. Aerosol and monsoon climate interactions over Asia. *Reviews of Geophysics*, 54(4): 866–929. doi: 10.1002/2015RG000500
- Menzel W P, Frey R A, Baum B A, 2013. *Cloud Top Properties and Cloud Phase Algorithm Theoretical Basis Document, Collection 006 Update*. Space Science and Engineering Center, 1–70.
- Menzel W P, Frey R A, Zhang H *et al.*, 2008. MODIS global cloud-top pressure and amount estimation: algorithm description and results. *Journal of Applied Meteorology and Climatology*, 47(4): 1175–1198. doi: 10.1175/2007JAMC1705.1
- Nakamura H, Oki M, Hayashi Y, 1985. A study on the estimation of the relative frequency of occurrences of the Clear Sky, the Intermediate Sky and the Overcast Sky in Japan. *Journal of Light & Visual Environment*, 9(2): 22–31. doi: 10.2150/jlve.9.2_22
- Pincus R, Platnick S, Ackerman S A *et al.*, 2012. Reconciling simulated and observed views of clouds: MODIS, ISCCP, and the limits of instrument simulators. *Journal of Climate*, 25(13): 4699–4720. doi: 10.1175/JCLI-D-11-00267.1
- Ramanathan V, Crutzen P J, Kiehl J T *et al.*, 2001. Aerosols, climate, and the hydrological cycle. *Science*, 294(5549): 2119–2124. doi: 10.1126/science.1064034
- Schiffer R A, Rossow W B, 1983. The international satellite cloud climatology project (ISCCP): the first project of the World Climate Research Programme. *Bulletin of the American Mete-*

- orological Society*, 64(7): 779–784. doi: 10.1175/1520-0477 (1991)072<0002:ICDP>2.0.CO;2
- Spena A D, D’Angiolini G, Strati C et al., 2010. First correlations for solar radiation on cloudy days in Italy. In: *ASME-ATI-UIT Conference on Thermal and Environmental Issues in Energy Systems*. Sorrento, Italy.
- Tang Q H, Leng G Y, 2013. Changes in cloud cover, precipitation, and summer temperature in North America from 1982 to 2009. *Journal of Climate*, 26(5): 1733–1744. doi: 10.1175/JCLI-D-12-00225.1
- U.S. Department of Commerce/National Oceanic and Atmospheric Administration, 1995. *Surface Weather Observations and Reports*. Federal Meteorological Handbook No.1. OFCM U.S. Department of Commerce/NOAA, 94. Washington, D.C.: U.S. Department of Commerce/National Oceanic and Atmospheric Administration.
- Wang F, Guo J P, Wu Y R et al., 2014. Satellite observed aerosol-induced variability in warm cloud properties under different meteorological conditions over eastern China. *Atmospheric Environment*, 84: 122–132. doi: 10.1016/j.atmosenv.2013.11.018
- Wang F, Guo J P, Zhang J H et al., 2015. Multi-sensor quantification of aerosol-induced variability in warm clouds over eastern China. *Atmospheric Environment*, 113: 1–9. doi: 10.1016/j.atmosenv.2015.04.063
- Warren S G, Eastman R M, Hahn C J, 2007. A survey of changes in cloud cover and cloud types over land from surface observations, 1971–96. *Journal of Climate*, 20(4): 717–738. doi: 10.1175/JCLI4031.1
- Wilson A M, Jetz W, 2016. Remotely sensed high-resolution global cloud dynamics for predicting ecosystem and biodiversity distributions. *PLoS Biology*, 14(3): e1002415. doi: 10.1371/journal.pbio.1002415
- Wu Jian, Liu Jia, 2013. Variations of cloud fraction over East Asia under global warming conditions in the past 20 years. *Journal of Tropical Meteorology*, 19(2): 171–180. doi: 1006-8775 (2013)02-0171-10
- Wylie D, Jackson D L, Menzel W P et al., 2005. Trends in global cloud cover in two decades of HIRS observations. *Journal of Climate*, 18(15): 3021–3031. doi: 10.1175/JCLI3461.1
- Xia X, 2012. Significant decreasing cloud cover during 1954–2005 due to more clear-sky days and less overcast days in China and its relation to aerosol. *Annales Geophysicae*, 30(3): 573–582. doi: 10.5194/angeo-30-573-2012